Supporting Information Appendix

Supplementary Methods

***Cep290* genotyping.**

Ear tissue was collected from F2 mice at P10 and genotyped for *Cep290* as previously described (19) using the following primers: F4, 5' -CATGTCTGCCTCCTTTAGTG- 3'; R2, 5' -GGCCTGCTCAAACCTGAAC- 3'; R5, 5' - CACTTCACATGGTATTGCTC- 3'. Tissues from mice homozygous for the gene trap allele were subsequently collected at P21; wild type littermates were also collected from some litters.

SNP genotyping.

Liver tissue was collected from *Cep290*$^{Gt/Gt}$ mice and snap-frozen in liquid nitrogen. Tissue was provided to NewGene Limited (www.newgene.org.uk) for DNA extraction and SNP genotyping using the MassARRAY system (Agena Bioscience). The primers used are available on request. Genotyping was initially validated using inbred 129/Ola mice, inbred C57BL/6 mice and F1 hybrid mice.

Genome-wide association analysis in mouse.

Standard quality control and association analysis of SNP genotype data from the genome-wide SNP panel was carried out using the software package PLINK (34) with visualisation (in the form of genome-wide Manhattan plots) carried out using the R package "qqman" (35). After removal of SNPs with low minor allele frequency and SNPs and mice with excessive amounts of missing data, each SNP was tested for association with phenotype via either linear regression (for the quantitative cystic index trait) or Fisher's exact test (for the binary coat colour traits), using a recessive coding of the SNP alleles in each case.

Whole exome sequencing of Joubert syndrome patients.

In brief, genomic DNA was isolated from blood lymphocytes and subjected to exome capture using Agilent SureSelect™ human exome capture arrays (Life technologies™) followed by next generation sequencing on the Illumina HiSeq™ sequencing platform. Sequence reads were mapped to the human reference genome assembly (hg19) using CLC Genomics Workbench™ (version 6.5.2) software (CLC bio, Aarhus, Denmark). Following alignment to the human reference genome, variants were called using GATK3 HaplotypeCaller and annotated vcf files were assessed using Qiagen Ingenuity software.

Variant filtration strategy of whole exome sequencing data.

Raw variant calls (in each vcf file) that did not meet any of the following criteria were filtered out using VCFtools (v 0.1.15): QUAL <10, DP < 4, QD < 2.0 or FS > 60.0. Variants located within the region of interest (chr1:43000000- 68000000) were identified and then annotated using Variant Effect Predictor (VEP) (v91). Variants common to two or more patients were identified by intersecting the variant calls using bcftools (v1.6).

Sequencing candidate SNPs via Sanger sequencing.

In *CEP290* ciliopathy patients where whole exome sequencing data was not available, genomic regions containing the SNPs of interest were amplified via PCR and sequenced via Sanger sequencing. Primers: rs2500341 FOR 5'-GGCAAGGAGTAAAGGTGGCT-3', REV 5'-ACATGCTCCAGATGATGCCC-3'; rs2253466 FOR 5'- GGAGCCAGACCTCGGTTTTG-3', REV 5'-CTGAGTGCCCGTAAAGGAGG-3'.

***In vivo* ASO Treatment of *Cep290*$^{Gt/Gt}$ Animals.**

In vivo ASO-based knockdown was performed on 28 day-old *Cep290*$^{Gt/Gt}$ and *Cep290*$^{+/+}$ animals as controls, as previously described (28). Briefly, knockdown of *Bsnd* was achieved using an octaguanidine dendrimer-modified antisense oligonucleotide morpholino (ASO) (GeneTools LLC, USA) designed to target the start codon of *Bsnd* 5'- CATTCGGCCCACGCTTACCTCTTTA -3'. ASO dissolved in PBS was injected into the tail vein of 28 day old *Cep290*$^{Gt/Gt}$ and *Cep290*$^{+/+}$ animals at a dose of 12.5 mg/Kg. 3 subsequent doses were administered at 3-4 day intervals over a period of 10 days, and tissues were collected 24 h after the final dose. Efficiency of the ASO was confirmed via western blot and immunofluorescence.

Tissue fixation and processing.

Murine kidneys and eyes were fixed in 4% paraformaldehyde (PBS) overnight at 4°C, then washed in PBS and dehydrated in 70% Ethanol. The tissue was processed into paraffin wax using a Shandon™ Pathcentre™ automatic processor (Thermo Fisher Scientific). Tissues were sectioned on a RM2235 microtome (Leica), at a thickness of 8 µm on to Polysine™ adhesion slides (Thermo Fisher Scientific). Murine brains were rinsed in PBS, fixed intracranially in 10% (vol/vol) neutral buffered formalin, and then stored at room temperature prior to processing.

Histological staining.

Slides were dewaxed in Histo-Clear II (National Diagnostics), then stained with Haematoxylin/Eosin (H+E), according to the following protocol. Slides were hydrated through a series of ethanol washes (100%, 90% 70% and 50%), rinsed in water, and then in Harris's haematoxylin for 1 minute. Slides were transferred into running tap water, differentiated with 1% acid alcohol and rinsed again in tap water. Slides were counterstained with 1% eosin for 30 seconds, rinsed in tap water, and then dehydrated. Slides were mounted in DPX mounting medium (Sigma-Aldrich) and visualised using a SCN400 Slide Scanner (Leica). For Masson's Trichrome, slides were dehydrated as stated above, and then re-fixed in Bouin's fixative for two hours at 56°C. Slides were cleared in running water then stained with Weigert's Iron Haematoxylin for 10 minutes, washed in water, stained in Biebrich Scarlet for five minutes and washed again. Slides were then placed in a mix of phosphotungstic and phosphomolybdic acid for five minutes then placed into Aniline Blue for a further five minutes. Finally, slides were washed in 1% acetic acid then rinsed in water and dehydrated, mounted and imaged (SI Appendix Figure S4) as stated above.

***Ex vivo* Magnetic Resonance Imaging.**

For cerebellar phenotyping a subset of mutant animals were analysed. Seven F2 mice with severe cystic kidney disease (cystic index >10%) and seven F2 mice with mild cystic kidney disease (cystic index <10%) were selected at random for brain imaging. Murine brains in 10% (vol/vol) neutral buffered formalin were transferred to a 10% (vol/vol) neutral buffered formalin solution containing 5 mM gadoteric acid (Dotarem, Gubert) for a period of 6 weeks to allow equilibration of the gadolinium-based T_1 contrast agent throughout the brain. Samples were removed from fixative solution, blotted dry, and immersed in a sealed cylindrical plastic container of perfluorotributylamine (a susceptibility-matched solution that does not contribute signal to an MR image). MR imaging of brain samples was performed on a 7T horizontal bore preclinical scanner (Varian Inc.) equipped with a 25-mm-diameter ^{1}H birdcage coil (Rapid Biomedical). Images were acquired using a T_1-weighted 3D gradient echo sequence (echo time = 9.5 ms, time repetition = 35 ms, field of view = 20.48 × 20.48 × 20.48 mm, acquisition matrix = 512 × 512 × 512), with a resultant isotropic image resolution of 40 μm. Six signal averages were acquired, resulting in an acquisition time of 15.3 h. Multiplanar reformatting of resultant datasets was performed using Horos (www.horosproject.org) to generate coronal, sagittal, and transverse views of brain structure.

Immunofluorescence imaging of murine kidney sections.

Samples were processed as previously described (28). Briefly, slides were dewaxed, rehydrated, boiled in citrate buffer (for antigen retrieval), washed and subsequently blocked in 10% foetal calf serum for 1 h. Slides were incubated overnight at 4°C in 2% foetal calf serum containing the following antibodies: rabbit anti-ARL13B (Proteintech, 17711-1-AP, 1:200), goat anti-Aquaporin 2 (Santa Cruz Biotechnology, sc-9882, 1:100), mouse anti-Barttin (Santa Cruz Biotechnology sc-365161, 1:100). Following washes in PBS, slides were incubated at room temperature for 90 min with the following secondary antibodies: donkey anti-rabbit Alexa Fluor 488 (Thermo Fisher Scientific, 1: 300), donkey anti-mouse Alexa Fluor 594 (Thermo Fisher Scientific, 1: 300), donkey anti-goat Alexa Fluor 647 (Thermo Fisher Scientific, 1: 300). Following final washes in PBS, slides were mounted in Vectashield (Vector Laboratories Ltd, H-1200). Images were captured in a blinded fashion, using an Axio Imager Z1 fluorescent microscope (Zeiss).

Immunofluorescence imaging of human kidney sections.

Immunofluorescence labelling of human kidney was performed on 4 µm thick paraffin 4% paraformaldehyde fixed sections, de-paraffinized and then boiled in citrate buffer (for antigen retrieval), pH 6.0 (2x5 min microwave at 900W). Non-specific binding sites were blocked with 1% BSA (PBS–0.1% Tween 20–1% BSA) followed by incubation in the same buffer overnight at 4°C with appropriate antibodies. Confocal images were taken using a spinning disc scanning microscope system (Yokogawa CSU-X1 spinning disk scanner coupled to a Zeiss Observer Z1 inverted microscope and controlled by Zen Blue software) with an X63.2 objective.

Image analysis.

Following capture, images were analysed using FIJI (ImageJ) software. To measure the size of the kidney cysts, three H&E images from each sample were thresholded using the colour threshold function and the size of cysts calculated using the measure particles function. The resulting sum of all of the cysts was then used to calculate the cystic index, correcting for the total size of the kidney. The length of cilia was measured using the segmented line tool on a maximum intensity projection of a *z*-stack. Cilia tortuosity was measured by summing the deviation from a straight line at every node on each segmented line measurement ($\Sigma\theta$).

Western blotting.

Kidney tissue was processed for western blot as previously described (28). Briefly, frozen kidneys were lysed in buffer containing 4 M urea, 125 mM Tris pH 6.8, 4% SDS, 10% glycerol, 5% β-

mercaptoethanol and 0.02% bromophenol blue. Protein samples were resolved by SDS-PAGE on a 4-20% gradient gel (Bio-Rad), and then transferred to a 0.4 µm nitrocellulose membrane (Thermo Fisher Scientific). The membranes were blocked in TBST (Tris-buffered saline, 0.1% Tween-20) containing 5% low fat milk for 1 h then incubated with the following primary antibodies in block overnight at 4 °C: mouse anti-Barttin (Santa Cruz Biotechnology sc-365161, 1:500), rabbit anti-GAPDH, (Cell Signaling technology, 2118, 1:5000). After washing in TBST, membranes were incubated with fluorescently labelled secondary antibodies (LI-COR) for 90 min at room temperature, washed again in TBST and visualized with an Odyssey CLx imaging system (LI-COR).

Supplementary Table S1.

Comparison of genotypes of SNPs in *BSND* and *TMEM61* and kidney involvement in patients with *CEP290* mutations.

Sample	Mutation1	Mutation2	Kidney Phenotype	Kidney disease Score[a]	rs2500341 MAF (C) 0.24	rs2253466 MAF (C) 0.39
213	c.5611_5614del; p.(Gln1871Valfs*2)	c.4882C>T; p.(Gln1628*)	Bilateral small hyperechogenic kidneys ESRD 9 years	High	GG	TT
373	c.4882C>T; p.(Gln1628*)	c.6072C>A; p.(Tyr2024*)	Left multicystic dysplastic kidney, right cystic kidney ESRD 6 years	High	CG	CT
412	c.1666dup; p.(Ile556Asnfs*20)	c.5344C>T; p.(Arg1782*)	Multiple medullary cysts, normal echogenicity CKD stage 4 age 10 years	High	GG	TT
441	c.5668G>T; p.(Gly1890*)	c.5356_5571del; p.(Glu1786_Leu1857del)	Multiple medullary cysts, hyperechogenic kidneys ESRD 24 years	High	GG	TT
455	c.1623+1G>A	c.5668G>T; p.(Gly1890*)	Bilateral small hyperechogenic kidneys ESRD 12 years	High	CG	CT
552	c.4723A>T; p.(Lys1575*)	c.4966G>T; p.(Glu1656*)	Multiple cysts in cortex and medulla of both kidneys CKD stage 1 at 4 years	High	GG	CT
AA	c.5668G>T; p.(Gly1890*)	c.5668G>T; p.(Gly1890*)	Small kidney cysts and loss of corticomedullary differentiation CKD stage 4 at 19 years	High	CC	TT
BB	c.2817G>T; p.(Lys939Asn)	c.2848insC; p.(Gln950Profs*6)	Hyperechogenic kidneys, corticomedullary cysts ESRD 4 years	High	GG	TT
F63	c.5668G>T; p.(Gly1890*)	c.4656delA; p.(Lys1552fs*1556)	Bilateral small hyperechogenic kidneys, ESRD 12 years	High	GG	TT
F394*	c.5668G>T; p.(Gly1890*)	c.5668G>T; p.(Gly1890*)	Enlarged cystic kidneys ESRD 12 years	High	GG	TT
F700*	c.5668G>T; p.(Gly1890*)	c.5668G>T; p.(Gly1890*)	Bilateral small hyperechogenic kidneys ESRD 11 years	High	GG	TT
F944*	c.5668G>T; p.(Gly1890*)	c.5668G>T; p.(Gly1890*)	Bilateral small hyperechogenic kidneys ESRD 13 years	High	GG	TT
G06	c.4966G>T; p.(Glu1656*)	c.2T>A; p.(Met1>Lys)	Multiple cysts in cortex and medulla of both kidneys ESRD age 20	High	GG	TT
H08	c.4174G>T; p.(Glu1392*)	c.4174G>T; p.(Glu1392*)	Bilateral small hyperechogenic kidneys ESRD 4 years	High	GG	CT
NPH3	c.5649-5650insA; p.(Leu1884fs*23)	c.5850delT; p.(Phe1950fs*15)	Bilateral small hyperechogenic kidneys ESRD 11 years	High	CC	CT
NPH4	c.5649-5650insA; p.(Leu1884fs*23)	c.5850delT; p.(Phe950fs*15)	Bilateral small hyperechogenic kidneys ESRD 19 years	High	CC	CT
NPH621	c.2915T>C; p.(Leu972Pro)	c.2915T>C; p.(Leu972Pro)	Bilateral small hyperechogenic kidneys ESRD 14 years	High	GG	TT
NPH966	c.2915T>C; p.(Leu972Pro)	c.2915T>C; p.(Leu972Pro)	Bilateral small hyperechogenic kidneys ESRD 16 years	High	CC	CC
717	c.5668G>T; p.(Gly1890*)	c2495_2512delInATCT; p.(Thr832Asnfs*12)	Loss of corticomedullary differentiation CKD stage 1 at 5 years	Low	CC	CT
C09	c.5932C>T; p.(Arg1978*)	c.5932C>T; p.(Arg1978*)	No kidney phenotype aged 9	Low	CG	CT
AD	c.297+1G>T	c.4661_4663delAAG; p.(Glu1553del)	No kidney phenotype aged 9	Low	CG	CT
LUW	c.6869_6870insA; p.(Asn2290Lysfs*6)	EX39_41del	No kidney phenotype aged 20	Low	CG	CT
LYW	c.6869_6870insA; p.(Asn2290Lysfs*6	EX39_41del	No kidney phenotype aged 13	Low	CG	CT
LA	c.2991+1655A>G	c.1709C>G; p.(Ser570*)	No kidney phenotype aged 6	Low	CG	CT
SS	c.2991+1655A>G	c.3310delinsAA p.Leu1104Asnfs*18)	No kidney phenotype aged 5	Low	CG	CT
HJ	c.2991+1655A>G	c.289G>T; p.Glu97*	No kidney phenotype aged 3	Low	CG	CT
B1106*	c.5668G>T; p.(Gly1890*)	c.5668G>T; p.(Gly1890*)	Hyperechogenic kidneys CKD stage 2, age 10	Low	CG	CT
F02*	c.5668G>T; p.(Gly1890*)	c.5668G>T; p.(Gly1890*)	Hyperechogenic kidneys CKD stage 1, age 15	Low	CG	CT
A1188*	c.5668G>T; p.(Gly1890*)	c.5668G>T; p.(Gly1890*)	Hyperechogenic kidneys CKD stage 1, age 11	Low	CG	CT

[a]Patients were scored based on their level of kidney function and the presence of cysts in the kidneys as shown by ultrasound. A high disease score indicates limited or no residual kidney function and/or the presence of multiple cysts within the kidney. *These data are shown in Table 1

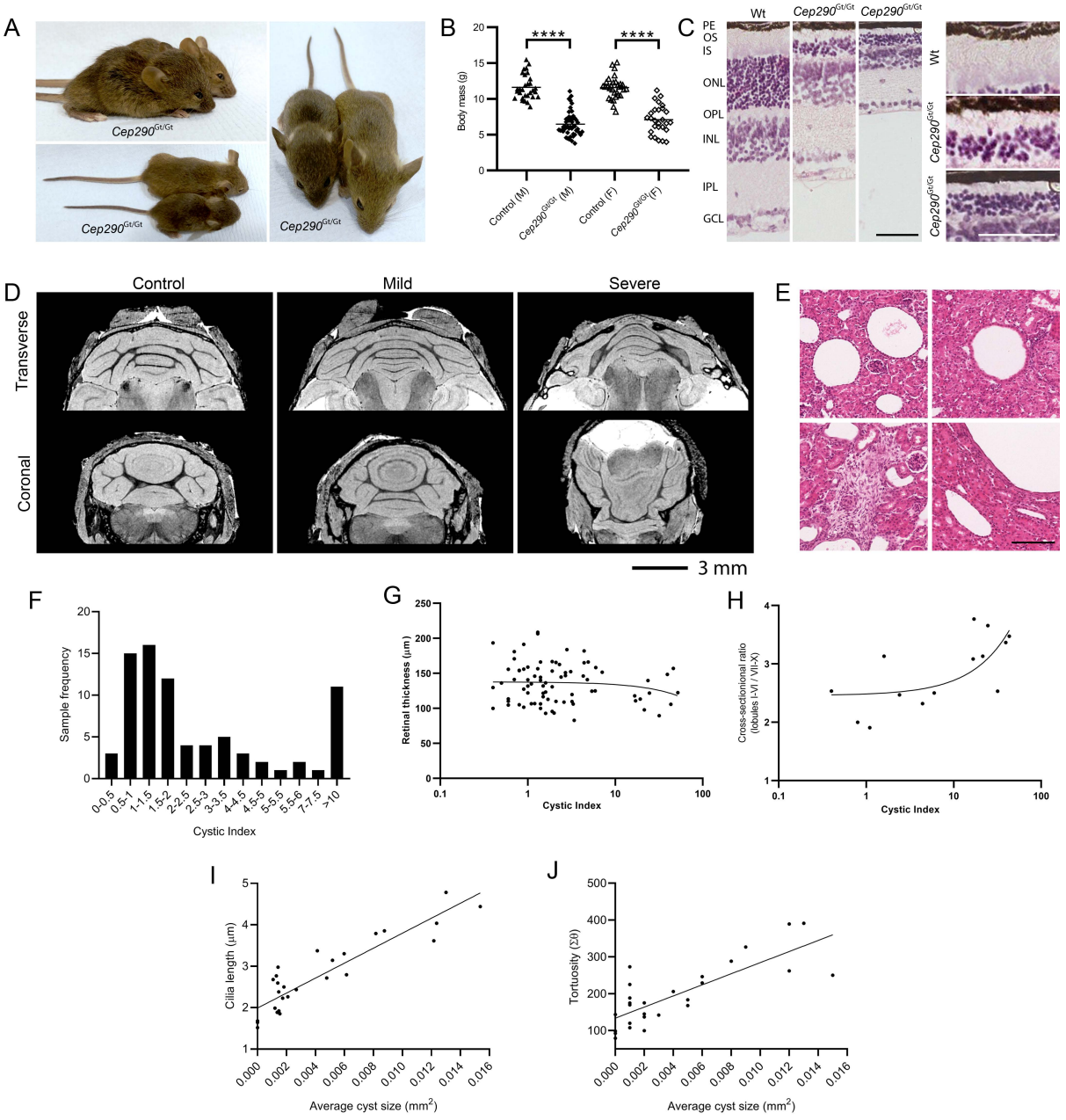

Figure S1

***Cep290*$^{Gt/Gt}$ F2 model demonstrates a cerebello-retinal-renal phenotype.**

(**A**) Postnatal day 21 (P21) *Cep290*$^{Gt/Gt}$ mice are reduced in size compared to their littermates, and display hydrocephalus and a shortened snout. (**B**) *Cep290*$^{Gt/Gt}$ mice are significantly smaller by mass at P21. This reduction in overall mass is observed in both males and females with no significant

difference within groups between males and females. (**C**) Haematoxylin and eosin (H&E) stained retinas from P21 wild-type and F2 *Cep290*$^{Gt/Gt}$ mice. *Cep290*$^{Gt/Gt}$ mice display a large degree of heterogeneity in the Outer nuclear layer (ONL), Outer plexiform layer (OPL), Inner nuclear layer (INL) and Inner plexiform layer (IPL); all Cep290$^{Gt/Gt}$ mice lack the outer segment of the photoreceptor layer. PE, pigmented epithelium; OS, Outer segment of the photoreceptor; IS, Inner segment of the photoreceptor. Scale bars 50 μm. (**D**) High resolution *ex vivo* MRI showing morphologically aberrant cerebellar structures in P21 F2 *Cep290*$^{Gt/Gt}$ mice. Coronal and transverse views reveal a substantial level of heterogeneity between mild and severe samples. (**E**) H&E histology of kidneys from severe F2 Cep290$^{Gt/Gt}$ mice. Cysts can be seen within the collecting ducts (upper left) and proximal convoluted tubules (upper right). Oedema is found to varying degrees in all samples (bottom left). In larger cysts within the collecting ducts, epithelial cells lining the cyst are particularly stretched and flat compared with smaller cysts (bottom right). (**F**) Histogram showing the distribution of the kidney phenotype in *Cep290*$^{Gt/Gt}$ mice. Mice predominantly have a low cystic burden (<5%) but a small subset have a substantially higher cystic burden ranging from 10-52%. **(G)** Scatter plot showing the absence of a link between the cystic index and overall retinal cellular loss in *Cep290*$^{Gt/Gt}$ animals. **(H)** Scatter plot showing loss of cells within the cerebellum is linked with increased cystogenesis in *Cep290*$^{Gt/Gt}$ animals ($R^2 = 0.42$, $P < 0.05$). (**I** and **J**) Scatter plots showing the average cyst size in *Cep290*$^{Gt/Gt}$ animals is strongly linked with cilia length (**I**, $R^2 = 0.82$, $P < 0.0001$) and cilia tortuosity (**J**, $R^2 = 0.63$, $P < 0.0001$).

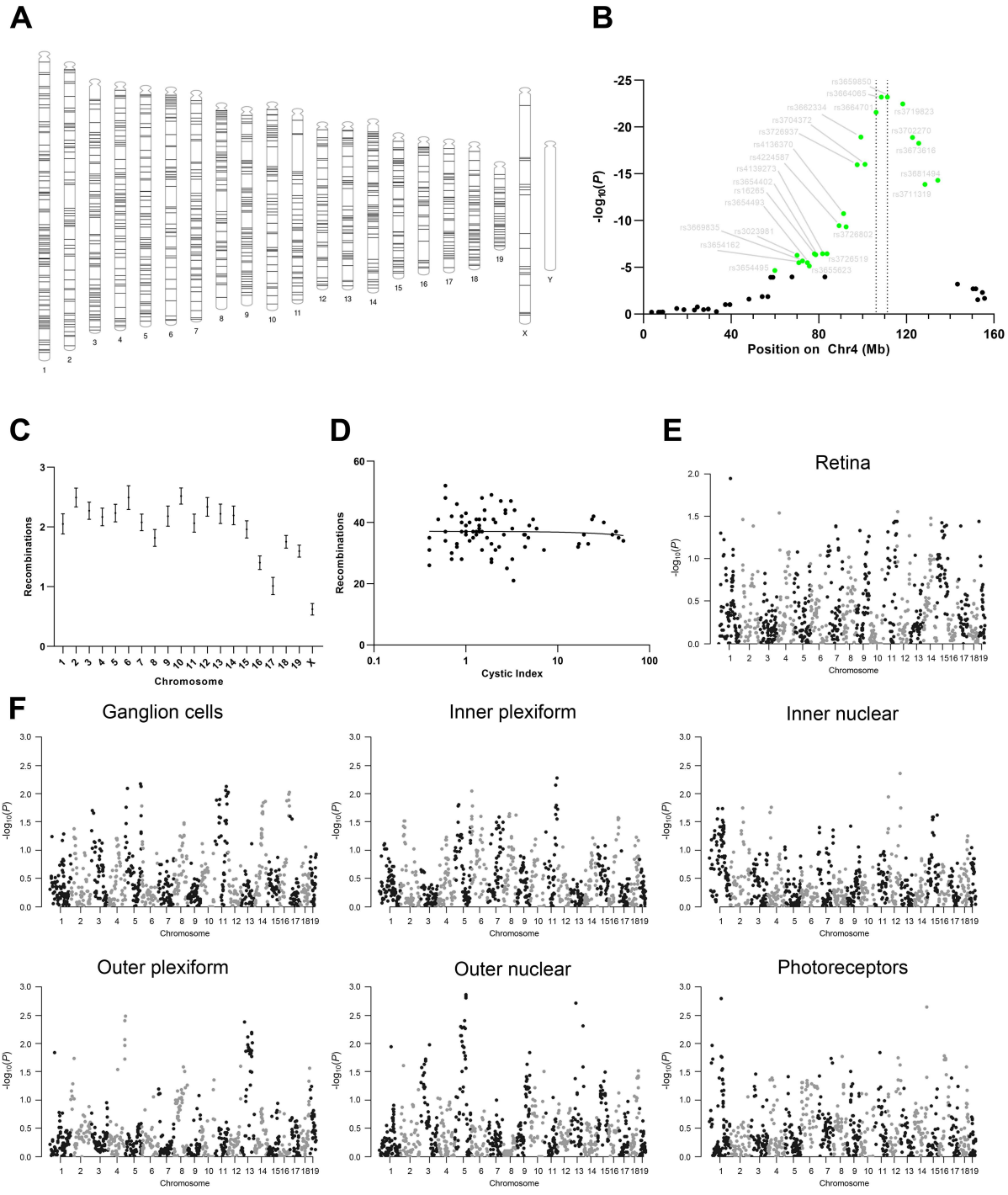

Figure S2

Genome wide association studies reveal a modifier locus which strongly affects renal pathophysiology but does not affect the retinal phenotype in *Cep290*$^{Gt/Gt}$ F2 mice.

(**A**) Ideogram, generated using Phenogram (https://ritchielab.org) showing the SNP locations used for genotyping C57BL/6 and 129/Ola alleles. **(B)** Scatter plot showing strength of association of each

variant in Chromosome 4 with cystic index. Variants shown in green are above the significance threshold ($6.34x10^{-5}$). All severe mice (Cystic Index >10%) were homozygous for SNPs originating from the C57BL/6 line in the region shown by the dotted lines. **(C)** Average number of recombination events in each chromosome across the sample cohort identified by SNP genotyping. **(D)** Scatter plot showing the total number of recombination events in each sample (Average of 39). No correlation between the number of recombination events and the cystic index were observed. (**E** and **F**) Manhattan plot showing strength of association of each variant with overall cellular loss within the whole retina (**E**) or specific layers within the retina (**F**) ordered according to genomic position. No SNPs were found to be significant (Significance threshold $P < 6.34X10^{-5}$).

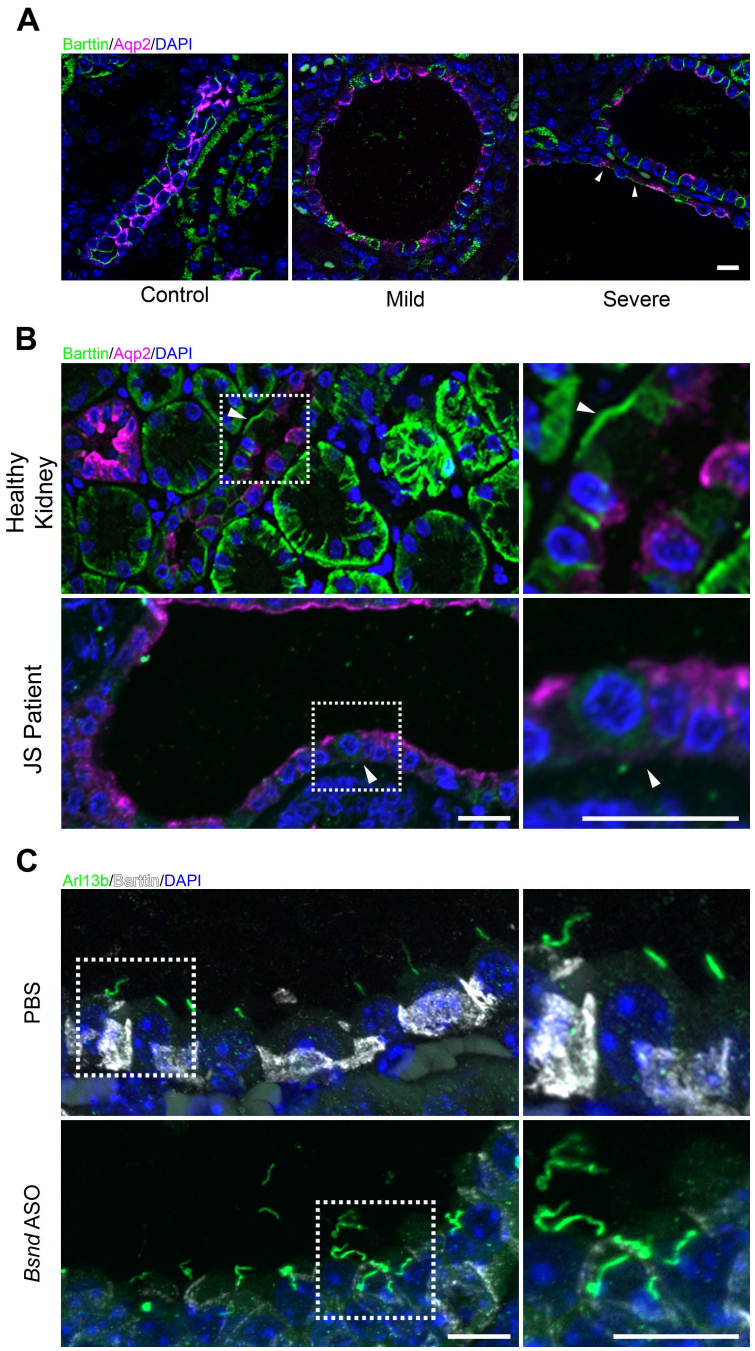

Figure S3

Loss of Barttin expression is linked to cystic kidney and abnormal primary ciliary phenotypes in murine F2 *Cep290*$^{Gt/Gt}$ model.

(**A**) Immunofluorescence staining of P21 mouse kidney from F2 *Cep290*$^{+/+}$ and *Cep290*$^{Gt/Gt}$ animals, showing the expression of Barttin (green) in intercalated cells, and Aquaporin 2 (Aqp2) (magenta) in

principal cells of the cortical collecting duct (CCD). Expression of both markers is observed in small cysts but is lost in larger cysts (arrow heads). Scale bar 10 µm. (**B**) Immunofluorescence images showing the expression of Barttin (green) and Aquaporin 2 (magenta) in a section of a kidney biopsy from a Joubert syndrome patient with end stage renal disease secondary to a mutation in *CEP290*. Basolateral Barttin expression is reduced in the patient sample (white arrow head).
(C) Immunofluorescence images of P21 mouse kidney from *Cep290*$^{Gt/Gt}$ animals on a 129/Ola background showing the expression of Arl13b (green) and Barttin (white) following injection of an antisense oligonucleotide targeted against *Bsnd*. Image shown in C is the same as in Figure 3C showing Barttin expression instead of Aqp2. Scale bars 10 µm.

Figure S4

Phenotypic series of F2 *Cep290*$^{Gt/Gt}$ murine kidneys.

Haematoxylin and eosin (H&E) histology of kidneys from whole cohort of F2 *Cep290*$^{Gt/Gt}$ mice.

Kidneys are ordered by cystic index from left to right and top to bottom. Scale bar 1 mm.

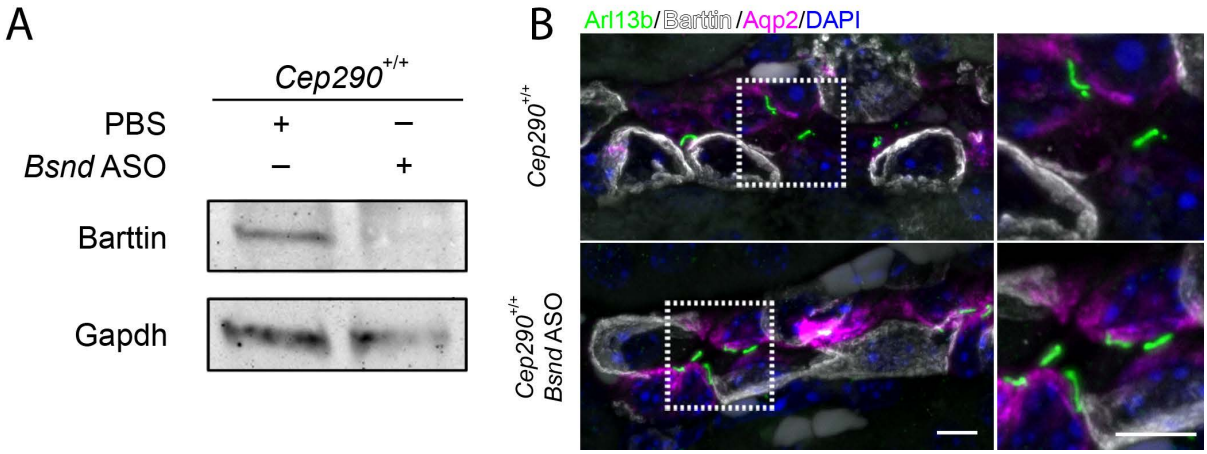

Figure S5

Loss of Barttin expression in *Cep290*$^{+/+}$ mice results in no ciliary phenotypic change.

(**A**) Western Blot showing reduction of Barttin protein level in wild type 129/Ola mice following knockdown with *Bsnd* ASO. (**B**) Immunofluorescence staining of P21 mouse kidney from 129/Ola *Cep290*$^{+/+}$ animals, showing the expression of Arl13b (green) in cilia, Barttin (white) in intercalated cells, and Aquaporin 2 (magenta) in principal cells of the cortical collecting duct (CCD). Expression of Barttin is reduced following knockdown with *Bsnd* ASO. No change in ciliary phenotype can be observed following knockdown of Barttin. Scale bars 5 µm.

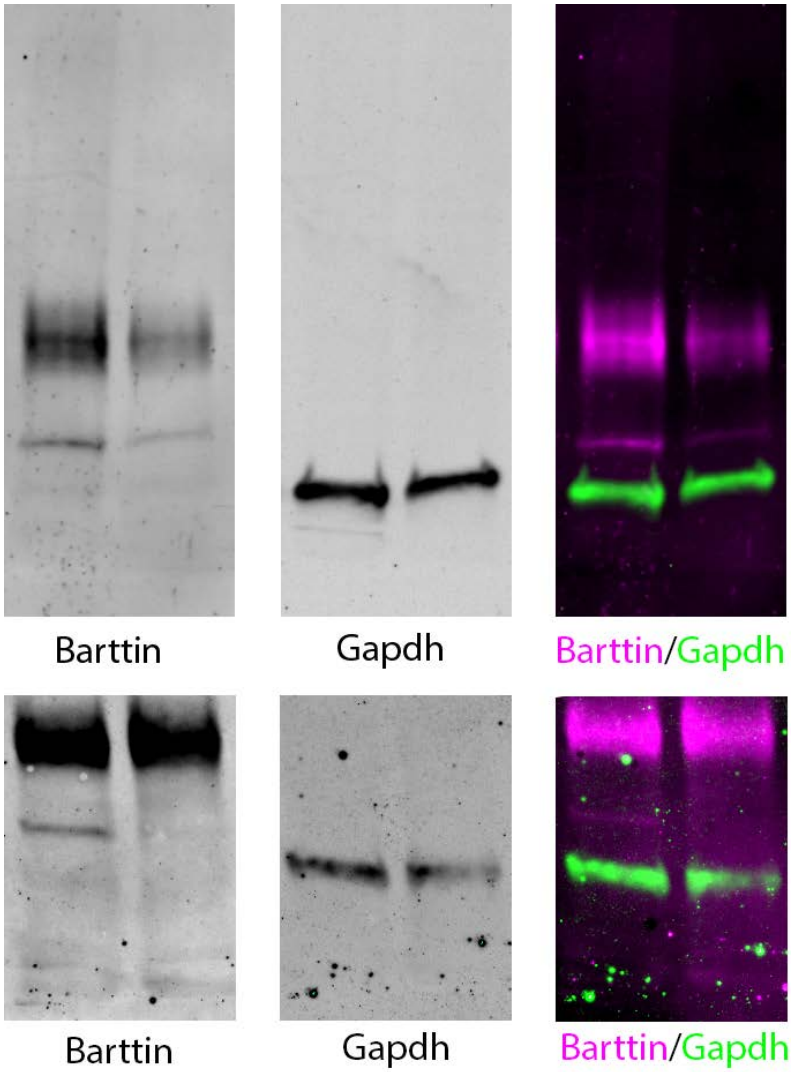

Figure S6

Uncut gel images from Figure 3B and Figure S5A